Journal of Experimental Botany, Vol. 72, No. 13 pp. 5079–5092, 2021
doi:10.1093/jxb/erab180 Advance Access Publication 4 May 2021

RESEARCH PAPER

Non-glandular trichomes of sunflower are important in the absorption and translocation of foliar-applied Zn

Cui Li[1,*], Jingtao Wu[2], F. Pax C. Blamey[2], Linlin Wang[1], Lina Zhou[1], David J. Paterson[3], Antony van der Ent[2], Victoria Fernández[4], Enzo Lombi[5], Yuheng Wang[1,*], and Peter M. Kopittke[2]

[1] School of Ecology and Environment, Northwestern Polytechnical University, Xi'an 710072, China
[2] School of Agriculture and Food Sciences, The University of Queensland, St Lucia, Queensland, 4072, Australia
[3] Australian Synchrotron, Clayton, Victoria, 3168, Australia
[4] School of Forest Engineering, Forest Genetics and Ecophysiology Research Group, Technical University of Madrid, 28040 Madrid, Spain
[5] Future Industries Institute, University of South Australia, Mawson Lakes, South Australia, 5095, Australia

* Correspondence: cui.li@nwpu.edu.cn or yuheng.wang@nwpu.edu.cn

Received 30 October 2020; Editorial decision 21 April 2021; Accepted 27 April 2021

Editor: Ann Cuypers, Hasselt University, Belgium

Abstract

Trichomes are potentially important for absorption of foliar fertilizers. A study has shown that the non-glandular trichromes (NGTs) of sunflower (*Helianthus annuus*) accumulated high concentrations of foliar-applied zinc (Zn); however, the mechanisms of Zn accumulation in the NGTs and the fate of this Zn are unclear. Here we investigated how foliar-applied Zn accumulates in the NGTs and the subsequent translocation of this Zn. Time-resolved synchrotron-based X-ray fluorescence microscopy and transcriptional analyses were used to probe the movement of Zn in the NGTs, with the cuticle composition of the NGTs examined using confocal Raman microscopy. The accumulation of Zn in the NGTs is both an initial preferential absorption process and a subsequent translocation process. This preferred absorption is likely because the NGT base has a higher hydrophilicity, whilst the subsequent translocation is due to the presence of plasmodesmata, Zn-chelating ligands, and Zn transporters in the NGTs. Furthermore, the Zn sequestered in the NGTs was eventually translocated out of the trichome once the leaf Zn concentration had decreased, suggesting that the NGTs are also important in maintaining leaf Zn homeostasis. This study demonstrates for the first time that trichomes have a key structural and functional role in the absorption and translocation of foliar-applied Zn.

Keywords: Foliar absorption, foliar fertilizers, translocation, trichome, sunflower, zinc.

Introduction

It has been known for more than two centuries that nutrients can be absorbed through plant leaves (Fernández *et al.*, 2013), and foliar fertilization has been used increasingly since the early 19th century (Griss, 1844). Recent research has examined the mechanisms by which foliar-applied nutrients move across the leaf surface, giving consideration to the roles of the

Abbreviations: DEG, differentially expressed gene; FPKM, fragments per kilobase of transcript per million mapped reads; GO, Gene Ontology;KEGG, Kyoto Encyclopedia of Genes and Genomes; NGT, non-glandular trichome; XFM, X-ray fluorescence microscopy; YFEL, youngest fully expanded leaf.

stomata, cuticle, and trichomes, although much uncertainty remains in this regard (Eichert *et al.*, 1998, 2008; Fernández *et al.*, 2017; Li *et al.*, 2018*a*, 2019). Non-glandular trichomes (NGTs) of sunflower (*Helianthus annuus*) have been reported to accumulate high concentrations of foliar-applied zinc (Zn) within 15 min (Li *et al.*, 2019). This observation suggests that for this plant species, trichomes potentially play an important role in the absorption of foliar fertilizers.

Trichomes are fine appendages on the leaf and stem surfaces that can be found in a variety of shapes and sizes and with varied cellular composition (Werker, 2000). They have been found to have multiple ecophysiological functions (Bickford, 2016), including resistance to herbivory (Levin, 1973; Dalin *et al.*, 2008), protection against UV radiation (Yan *et al.*, 2012), and production of specialized metabolites (Schilmiller *et al.*, 2008). Furthermore, trichomes of some species have been reported to play an important role in foliar water uptake (Pina *et al.*, 2016), and this may be related to the foliar absorption of solutes observed previously (Li *et al.*, 2019). Foliar water uptake through leaf trichomes has been reported, for example, for epiphytic bromeliads that do not have functional roots (Benzing *et al.*, 1976; Ohrui *et al.*, 2007; Martin *et al.*, 2013; Herppich *et al.*, 2019) and in dry environments as an adaptation to acquire water from the environment (Pina *et al.*, 2016; Holanda *et al.*, 2019; Schreel *et al.*, 2020). At least 11 species representing six different plant families had been reported to have leaf trichomes that are important for foliar water uptake (see Supplementary Table S1 for the full list) (Ju *et al.*, 2012; Fernández *et al.*, 2014; Vitarelli *et al.*, 2016; Schreel *et al.*, 2020).

Despite the importance of trichomes in foliar water uptake and the potential importance of trichomes in absorption of foliar fertilizers, the mechanisms whereby foliar-applied Zn accumulates rapidly in the NGTs remain unclear. In addition, the fate of foliar-applied nutrients after their initial accumulation within the trichomes is also unclear in terms of whether they remain in the absorbing trichomes or if are translocated to other plant tissues. In this regard, few studies have utilized transcriptome analyses to examine leaf trichomes (Hunt *et al.*, 2011; Balcke *et al.*, 2017), but, to the best of our knowledge, no previous study has implemented transcriptome analyses to examine leaf trichome responses to foliar-applied nutrients. Such information would be important for deciphering the mechanisms regulating the absorption and translocation of foliar-applied nutrients.

In the present study, using sunflower as a model species, we focused on the foliar absorption of Zn in the NGTs and its subsequent translocation. The questions that we aimed to answer were: (i) is the foliar-applied Zn that accumulates within the NGTs absorbed directly by the NGTs, or is it translocated to NGTs following rapid absorption by other epidermal components; and (ii) what is the subsequent fate of the Zn absorbed by the NGTs—does it remain in the NGTs or is it transported to other tissues? To answer these questions, we utilized time-resolved, *in situ* synchrotron-based X-ray fluorescence microscopy (XFM) to trace the movement of Zn following its foliar application in living plants. Furthermore, based upon these results from XFM, NGTs were collected at different time intervals during the translocation process for transcriptome analysis. Confocal Raman microscopy was then utilized for *in situ* comparison of the cuticle covering the NGT bases with that of the cuticle covering leaf epidermal cells. The structure of NGTs was also examined using TEM. Our results provide new insights into the role that trichomes play in absorption and translocation of foliar-applied Zn, and potentially allow the development of more efficient foliar fertilization practices.

Materials and methods

Plant growth and Zn foliar fertilizer

Sunflower plants were grown in controlled environments as described by Li *et al.* (2018*b*). Briefly, sunflower (cv. Hyoleic 41) seeds were germinated in a moistened paper towel for 4 d. The seedlings were transferred to 11 litre black containers that were filled with nutrient solution containing (μM): 910 N (94% NO_3^- and 6% NH_4^+), 475 K, 20 P, 1126 Ca, 227 Mg, 1251 Cl, 556 S, 25 Fe(III)EDTA, 3 B, 0.5 Mn, 0.5 Zn, 0.2 Cu, and 0.01 Mo (Blamey *et al.*, 2015). The nutrient solutions were continuously aerated and were changed weekly. After growing in the containers for 10 d, 5 ml of 44 mM KH_2PO_4 was added every second day thereafter to replenish the P being taken up by plants. Each container had four plants. Light was provided using high-pressure sodium lamps (photon flux density of 1500 μmol m^{-2} s^{-1}) for 12 h d^{-1}. The temperature was maintained at 25 °C. After 2 or 3 weeks (see below), the youngest fully expanded leaves (YFELs) were then utilized for the various experiments, as outlined below.

The foliar Zn fertilizer used in the present study was a 1000 mg l^{-1} Zn solution (15.4 mM, pH 5.2) prepared using $ZnSO_4 \cdot 7H_2O$, with the solution containing 0.05% Tween-20 as a surfactant (Reuveni *et al.*, 1994).

Distribution of Zn in the leaves

The distribution of Zn in the leaves was mapped by XFM analysis conducted at the XFM beamline of the Australian Synchrotron (Clayton, Australia). Plants grown at The University of Queensland were transported to the Australian Synchrotron where they continued to be grown there under the same conditions until being analysed over a period of 5 d. Two broad types of samples were examined. Some leaves were examined after being excised, whilst other leaves were examined whilst still attached to living plants—the latter allowing for time-resolved analyses of changes in Zn distribution in a living plant following foliar fertilization. The foliar application of the Zn and sample preparation methods for the XFM analyses were similar to those described by Li *et al.* (2018*a*).

We first examined excised leaves of 3-week-old plants to which 5 μl (i.e. a single droplet) of the Zn solution was applied to a YFEL whilst the leaf was still attached to the plant. Immediately thereafter, the leaf was sealed in a Petri dish (whilst remaining attached to the plant) to prevent the droplet from drying. After 0.5 h, the droplet was blotted dry with filter paper before the leaf was excised and rinsed thoroughly using 3% ethanol, 2% HNO_3, and deionized water (Vu *et al.*, 2013). A second YFEL served as a control to which a droplet of 5 μl of deionized water containing 0.05% Tween-20 had been applied. After 0.5 h, this control leaf was also rinsed and examined. The two leaves (control and Zn treated) were placed on a sample holder, completely sealed using two pieces of 4 μm thick Ultralene film to keep the excised leaves hydrated, and analysed using XFM.

The XFM analysis was conducted with an excitation energy of 12 900 eV. The X-rays were selected using an Si(111) monochromator and the beam size was 2 μm×2 μm. A 384-element Maia detector system in a backscatter position was used to collect the X-ray fluorescence emitted by the specimen (Kopittke *et al.*, 2011; Paterson *et al.*, 2011). The total photon flux was ~ 2.9×10^9 photons s^{-1} on the sample. For each specimen, a quick survey scan was first conducted to locate the area to which the droplet had been applied, with this then being the area where a detailed scan was conducted. For this initial survey scan, the step size was 30 μm with a horizontal stage velocity of 5 mm s^{-1}, resulting in a pixel transit time of 6 ms. Next, the detailed scan was used to more closely examine the distribution of Zn in the NGTs and the surrounding tissues. The step size was 2 μm with a horizontal stage velocity of 1.5 mm s^{-1}, resulting in a pixel transit time of 1.33 ms. All images presented in this study are from the detailed scans. Data were analysed using GeoPIXE (Ryan and Jamieson, 1993; Ryan, 2000).

Next, we utilized XFM to examine leaves attached to living plants. For these time-resolved analyses, an intact 2-week-old plant was transferred to a 50 ml centrifuge tube. The tube was filled with nutrient solution and the stem was held firmly in place to prevent movement. A 100 μl droplet of the Zn solution was applied for 0.5 h before being removed by blotting dry with filter paper. This leaf was then mounted as flat as possible on the sample holder (Supplementary Fig. S1) but not enclosed in Ultralene to ensure that transpiration was not inhibited. The leaf was then repeatedly scanned at the same location at seven intervals (0.25, 2.2, 4, 6, 20, 45, and 60 h) after the excess Zn had been removed from the leaf surface. At each of these time intervals, a survey scan was first used to find the location where the Zn had been applied, with detailed scans (~4 megapixels each) then conducted. These detailed scans were conducted in the same areas after each time interval to examine changes in Zn distribution over time. The parameters of the survey and detailed scans were the same as above. Each survey scan took ~3 min whilst each detailed scan took ~50 min. The nutrient solution in the tube was refreshed daily and the plant was maintained in the normal lighting cycle except during XFM analysis. The plant and the leaf were visually examined after the analysis. Two living plants were examined separately, these being two replicates. The two replicates were consistent with each other; hence only one set of results is presented.

Composition of the leaf cuticle and the base of NGTs

The YFELs of 3-week-old plants were excised at the petiole and immediately examined by confocal Raman microscopy (alpha 300R, WITec). A ×50 objective (Zeiss LD EC Epiplan-Neofluar Dic 50×/0.55) was used to focus the laser onto either a general region of the leaf where trichomes are absent (henceforth referred to as a 'general cuticular area') or the base of an NGT on the adaxial leaf surface, with the diameter of the beam being 0.8 μm. The wavelength of the laser was 532 nm and the laser power on the sample was 1 mW. The Raman light was detected by a spectroscopic CCD sensor. Spectra were collected for 15 s over the range of 0–2000 cm^{-1} (Gierlinger and Schwanninger, 2006; Yu *et al.*, 2007). A camera was connected to take photographs of the area being analysed. Three replicate analyses were conducted, with the data plotted using Origin® 2019b after being baseline corrected and normalized to [0,1].

Structure of the NGTs

The YFELs of 3-week-old plants were cut into 1 mm×3 mm segments and fixed in 2.5% glutaraldehyde in 0.1 M phosphate buffer (pH 7.2–7.4) for 2 weeks. The segments were then rinsed four times using 0.1 M phosphate buffer and post-fixed with 1% OsO_4 in 0.1 M phosphate buffer overnight before being rinsed four times with 0.1 M phosphate buffer. Samples were dehydrated in an ethanol series of 30, 50, 70, 80, 90, and 100%, with each concentration being used for 10 min and with each step repeated twice. The samples were then infiltrated with LR white resin in ethanol as follows: 25% for 2 h, 50% for 8 h, 75% for 12 h, and 100% for 24 h, with each step repeated twice. Next, the samples were embedded with 100% LR white in blocks and polymerized at 60 °C for 48 h. Sections (70 μm) were then cut using an ultramicrotome (LEICA EM UC6), with the sections then placed on a carbon-coated copper grid and stained with uranyl acetate for 10 min and lead citrate for 5 min (rinsing with deionized water after each stain). The samples were then examined using TEM (FEI, Themis Z) at 300 kV. Light micrographs of the cross-sections were collected using an Aperio XT Slide Scanner after the fresh leaf was sectioned using a vibratome (Leica VT 1000s). SEM was used to examine the sunflower leaf surface, using a JEOL NEOSCOPE SEM at 10 kV as detailed by Li *et al.* (2019).

Time-resolved transcriptome analysis of gene expression in NGTs

Trichome collection

Based on the XFM analyses (see the Results), it was found that the Zn concentration in the NGTs had already increased by the end of the 0.5 h Zn application period, and then (despite the Zn having been removed from the leaves) continued to increase until 6 h, with the Zn concentration in the NGTs then decreasing thereafter. To examine Zn translocation in the NGTs at a molecular level, the NGTs of the adaxial leaf surface of the following three treatments were collected: control leaves (T0); leaves to which Zn had been applied for 0.5 h and then the excess Zn solution was removed from the leaf surface (T1); and leaves to which Zn had been applied for 0.5 h before the excess was removed, with the leaves then allowed to continue growing for a further 45 h (T2). For these treatments, plants were grown for 2 weeks in the same conditions as described previously. Deionized water was then applied to T0 and Zn was applied to T1 and T2. In all instances, the relevant solutions were sprayed over the entire adaxial surface of the YFELs, with the solutions removed by blotting dry with filter paper after 0.5 h. The NGTs on the adaxial surface were immediately removed at their base using fine tweezers (0.1 mm) under a light microscope. It took up to 3 h to remove the trichomes. During collection, the trichomes were put into an RNase-free tube on ice. Upon completion, the tube was immediately frozen in liquid nitrogen and placed in a freezer (–80 °C) until further analysis. Three replicates of each sample were collected. Each sample weighed ~0.2 g and was collected from at least four YFELs.

RNA sequencing, data filtering, and mapping

The RNA of the NGT samples was extracted and 1% agarose gels were used to check the degradation and contamination of the RNA, with a NanoPhotometer spectrophotometer (IMPLEN, CA, USA) used to check purity, and an RNA Nano 6000 Assay Kit of the Bioanalyzer 2100 system (Agilent Technologies, CA, USA) used to check the integrity. For each sample, 1 μg of RNA was used to generate the RNA sequencing (RNA-Seq) libraries utilizing the NEBNext Ultra RNA Library Prep Kit for Illumina (Novogene, Beijing, China) (Yue *et al.*, 2018). In order to select cDNA fragments that were 250–300 bp, the libraries were purified using the AMPure XP system (Beckman Coulter, Beverly, MA, USA). The library quality was assessed using the Agilent Bioanalyzer 2100 system. The clustering was performed using a cBot Cluster Generation System with the TruSeq PE Cluster Kit v3-cBot-HS (Illumia). It was then sequenced on an Illumina Novaseq platform and 150 bp paired-end reads were generated.

Reads of low quality and containing adapter or poly-N were removed from the raw reads to produce the clean reads, with the Q20, Q30, and GC content of the clean data also calculated. All the analysis was performed using the processed clean reads. The clean reads were aligned to the genome of sunflower using Hisat2 v2.0.5 (Badouin *et al.*, 2017).

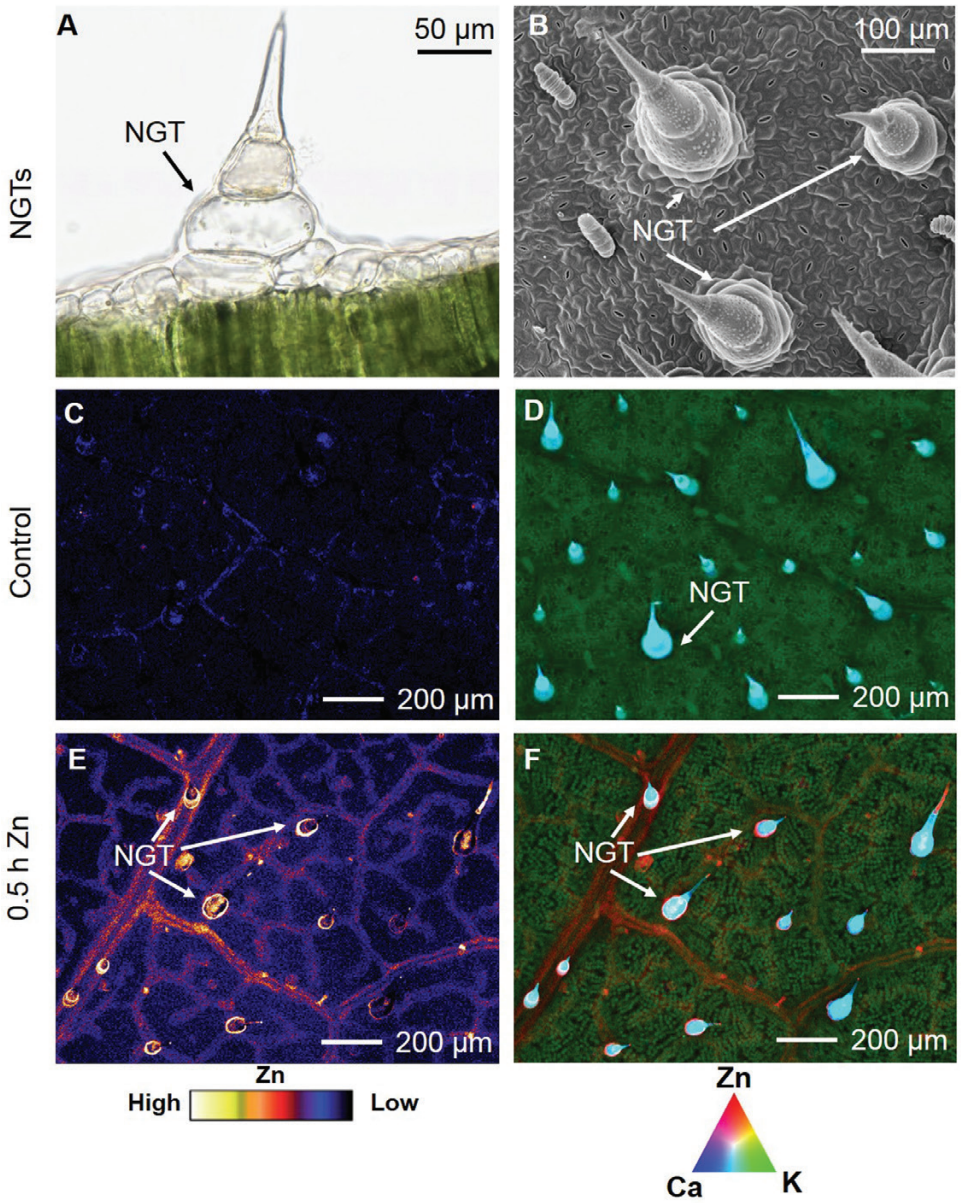

Fig. 1. Light micrograph (A) of a cross-section of a sunflower leaf. Scanning electron micrograph (B) of the adaxial surface of the leaf showing the non-glandular trichomes (NGTs). (C–F) The XFM images showing Zn distribution in sunflower leaves, with (C) and (D) being for the control leaf and (E) and (F) being for a leaf to which Zn had been applied for 0.5 h before being excised. The colours are comparable in (C) and (E), with brighter colours showing higher Zn concentrations. In (D) and (F), red shows Zn, green shows K, and blue shows Ca.

Gene expression analysis

For quantification of the gene expression level, featureCounts v1.5.0-p3 was employed to count the read numbers mapped to each gene, then fragments per kilobase of transcript per million mapped reads (FPKM) of each gene were calculated based on the length of the gene and read counts mapped to this gene (Nautiyal *et al.*, 2020). The differentially expressed genes (DEGs) between the three samples were analysed using the DESeq2 R package. Genes with an adjusted *P*-value ≤0.05 and $|\log_2$ (foldchange)$|$ ≥0 found by DESeq2 were assigned as differentially expressed.

Gene Ontology and pathway analysis of the differentially expressed genes

Gene Ontology (GO) analysis was used to classify the functions of the DEGs between samples, with the DEGs classified as biological process (BP), cellular component (CC), and molecular function (MF). The Kyoto Encyclopedia of Genes and Genomes (KEGG) is a database which elucidates the molecular interactions among the genes. GO enrichment and the KEGG analysis of the DEGs between the samples were conducted using the clusterProfiler R package (3.4.4) with the adjusted *P*-value <0.05 to identify significantly enriched GO terms and biological pathways.

qRT–PCR validation

To verify the differential expression of the DEGs identified in our transcriptome data, 15 genes were randomly selected for quantitaive real-time reverse transcription–PCR (qRT–PCR) analysis, and the actin and ubiquitin genes were used as the internal controls (Fernandez *et al.*, 2008; Ramu *et al.*, 2016). The primers used for qRT–PCR are listed in Supplementary Table S2. Three replicate samples of trichomes were

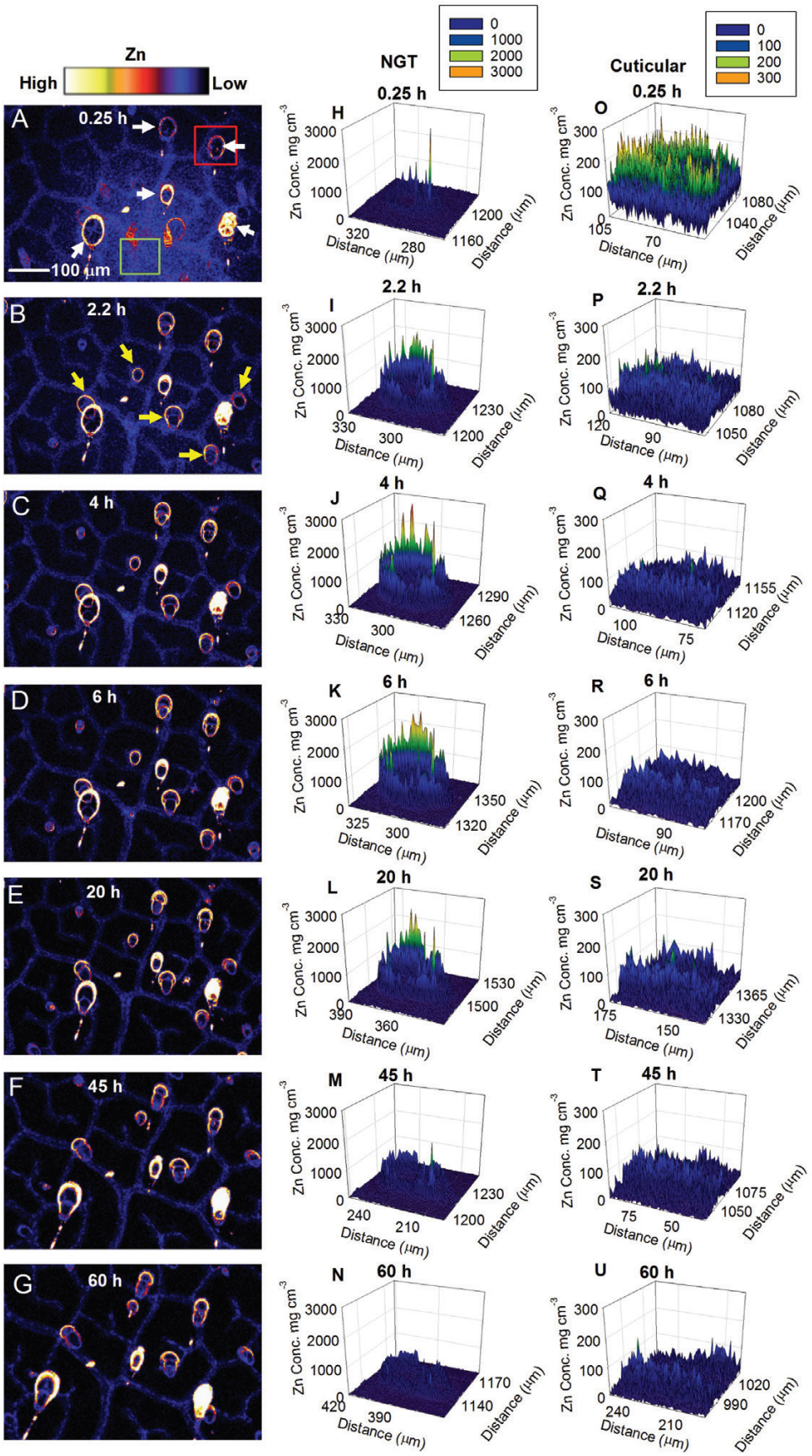

Fig. 2. Results of time-resolved XFM showing changes in Zn distribution in a leaf to which Zn had been applied for 0.5 h prior to examination. The entire area shown was underneath where the droplet had been applied. (A–G) Detailed scans of the same leaf area conducted at 0.25, 2.2, 4, 6, 20,

collected as above and the total RNA extracted. The first-strand cDNA was synthesized by the Prime Script® RT reagent Kit (Takara). The primers were designed using Primer3 (v. 0.4.0). The qRT–PCR was performed using a SYBR Premix EX Taq Kit (Takara) in a 20 µl reaction mixture on an ABI7300 (Applied Biosystems, Foster City, CA, USA). The relative expression levels was assessed using the $2^{-\Delta\Delta CT}$ method (Livak and Schmittgen, 2001).

Results

Distribution and movement of foliar-absorbed Zn in sunflower leaf NGTs

The NGTs are one of the three types of trichomes present on sunflower leaves (Aschenbrenner *et al.*, 2013), being the largest trichome in size and having a density of 880 cm^{-2} [(Fig. 1A, B), see Li *et al.* (2019) for more information regarding the NGTs]. The XFM analyses showed that the Zn concentration within the leaf tissues had already begun to increase after 0.5 h of the foliar application treatments (Fig. 1C, E). Furthermore, Zn accumulated within both the general cuticular areas and in the NGTs, especially in the basal areas of the NGTs (Fig. 1E, F). This is in contrast to the control leaf in which neither the general cuticular areas nor the NGTs were found to have increased Zn concentrations (Fig. 1C, D). It is important to note that XFM is not a surface-sensitive approach for Zn at the K-edge due to its comparatively high energy (8.6 keV), hence it is possible to detect Zn across the entire thickness of the leaf.

To further examine the movement of Zn in the NGTs following its foliar absorption, time-resolved XFM analyses were used to observe changes in Zn concentration over time in a leaf of a living plant. Firstly, after the 0.5 h exposure period had been completed, it was noted that the Zn concentration of the general cuticular areas gradually decreased over time, as indicated by decreasing colour brightness (Fig. 2A–G). This indicated that the Zn had initially accumulated in these areas following foliar fertilization and was then progressively moved away. However, a different pattern was observed for the NGTs—especially for the basal areas where Zn concentrations increased over time before then decreasing after 6 h (Fig. 2A–G). Interestingly, at 0.25 h, and especially at 2.2 h, Zn was present not only in the NGTs on the adaxial leaf side (i.e. the surface where the Zn had been applied) but also in those on the abaxial surface (see the white and yellow arrows in Fig. 2A, B and Supplementary Fig. S2 for an explanation). This indicates the base of the NGTs to be a preferred accumulation site for foliar-absorbed Zn, with Zn rapidly translocating into the base of the abaxial NGTs.

Next, a specific NGT and a general cuticular area were selected (Fig. 2A) to quantify the Zn concentration of these areas using a three-dimensional representation (Fig. 2H–N for the NGT and Fig. 2O–U for the general cuticular area). After 0.25 h, the average Zn concentration in the NGT was ~300 µg cm^{-2} (Fig. 2H) whilst it was ~100 µg cm^{-2} in the general cuticular area and 200 µg cm^{-2} in the leaf vein (Fig. 2O). However, these concentrations changed over time. For the NGT, the average concentration increased from 300 µg cm^{-2} (0.25 h) to ~1000 µg cm^{-2} (6 h) before then decreasing to ~300 µg cm^{-2} (60 h, Fig. 2H–N). In contrast, Zn in the general cuticular area decreased gradually after 0.25 h to ~20 µg cm^{-2} after 60 h. A similar pattern of decrease occurred in the vein, decreasing to 60 mg cm^{-3} after 60 h (Fig. 2O–U). These observations indicate that the base of the NGTs seemed to have a higher absorption rate for foliar-applied Zn, with further accumulation of Zn in the NGTs over the subsequent 6 h before then being progressively translocated elsewhere.

In situ *estimation of epidermal surface composition of the general cuticular area versus the NGT basal area*

Using *in situ* analyses, the composition of the cuticle was examined for both the general cuticular area and the NGT basal area (Fig. 3). The three replicate analyses are similar, and hence only one replicate is shown. Based upon previous studies (Yu *et al.*, 2007), the small peaks at 962, 1001, and 1186 cm^{-1} were ascribed to the vibration of δ(CC) ring breathing, with this being associated with the triterpenoids in the cuticle. The strong peaks at 1155 cm^{-1} (C–C single-bond stretching) and at 1520 cm^{-1} (C=C stretching) are likely to be from carotenoid pigments (Greene and Bain, 2005; Schrader *et al.*, 2005). A notable distinction between the NGT basal area and the general cuticular area is that the NGT base had a pronounced peak at 1080 cm^{-1}, with this being assigned to ν (CO), which is probably related to carbohydrates in the cuticle at the base of the NGT (Gierlinger, 2018).

Structure of the NGTs from TEM

Examination of NGTs using TEM showed that the epidermal cells of the general cuticular area and the basal cells of the NGT did not differ markedly in regard to the thickness of the combined cuticle and cell wall (Fernández *et al.*, 2016), with both having a thickness of ~1.8 µm (Fig. 4A, B). Interestingly, plasmodesmata connected the NGT basal cell to the adjacent epidermal cell (Fig. 4C) as well as the underlying mesophyll cell (Fig. 4D).

45, and 60 h after 0.5 h foliar Zn application, with colours being comparable between images and with brighter colours corresponding to higher Zn concentrations. (H–N) Three-dimensional representations of the Zn concentration extracted from (A–G) for the NGT indicated by the red box in (A). (O–U) Three-dimensional representations of the Zn concentration extracted from (A–G) for the general cuticular area indicated by the green box in (A). The white arrows in (A) indicate NGTs on the adaxial leaf side and the yellow arrows in (B) indicate the NGTs on the abaxial leaf side. The scale bar in (A) applies to (A–J). The key in (H) applies to (H–N) and the key in (O) applies to (O–U). Note the different scales of the *y*-axis in (H–N) and (O–U).

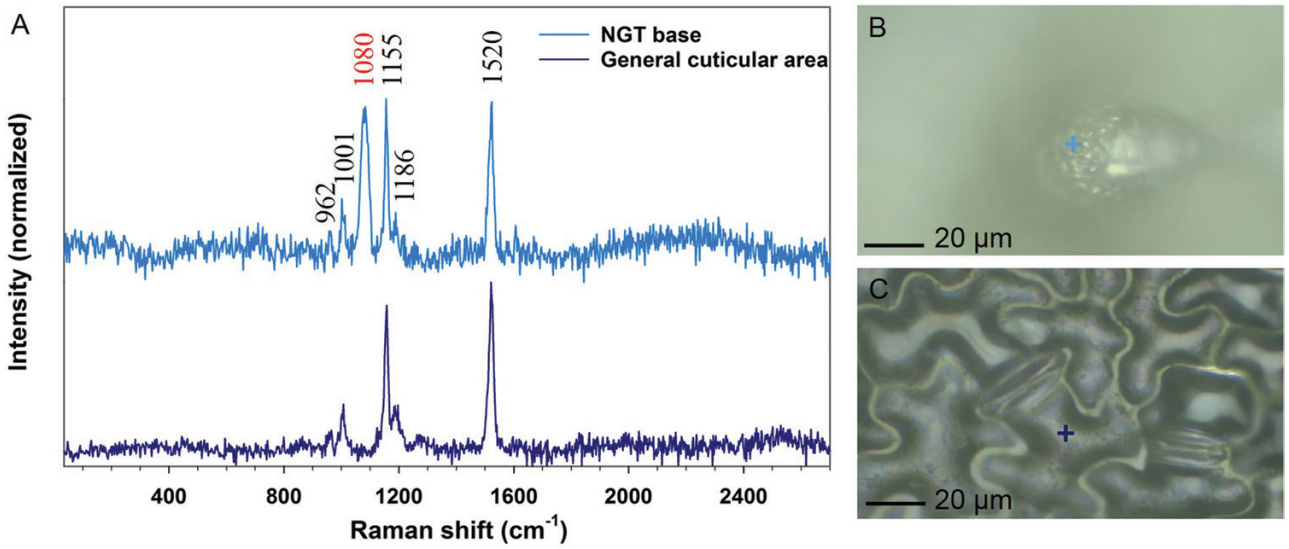

Fig. 3. The composition of the cuticle in the general cuticular area and the NGT basal area. (A) Raman spectra of the NGT base and the general cuticular area of the adaxial surface of a sunflower leaf in the 35–2700 cm^{-1} spectral region. Optical micrographs showing (B) the NGT base and (C) the cuticular area, with the 'plus' (+) symbol indicating the area where the analysis was undertaken.

Identification of DEGs in the NGTs of different Zn translocation patterns

Based on the XFM analyses, NGTs were collected for transcriptome analysis at the following times: (i) T0 as the control; (ii) T1 representing Zn translocation into the NGTs; and (iii) T2 representing Zn translocation out of the NGTs. The high-throughput Illumina sequencing yielded an average of 44.8 million clean reads from T0, 44.3 million from T1, and 42.7 million from T2 (Supplementary Table S3). After aligning to the sunflower genome, T0 had a unique alignment rate of 73.3%, T1 of 82.4%, and T2 of 81.1% (Supplementary Table S4). In addition, the Spearman correlation coefficient between the biological replicates of the three samples varied from 0.83 to 0.96, indicating good quality of the replicates (Supplementary Table S5). Next, the expression levels of these genes from the uniquely mapped libraries were normalized as FPKM (see the full list of the FPKM value of the genes in Supplementary Table S6). As shown in Fig. 5, compared with T0, a total of 8561 genes were differentially expressed in T1, with 4989 genes up-regulated and 3572 genes down-regulated; a total of 6460 genes were differentially expressed in T2, with 3838 up-regulated and 2621 down-regulated (Supplementary Table S7). Compared with T1, T2 had a total of 3831 DEGs, with 1636 up-regulated and 2175 down-regulated. These results indicate that the gene expression of the NGTs was significantly influenced by foliar Zn application.

GO and KEGG metabolic pathway analysis of the DEGs

To further evaluate functional differences in the DEGs between the three samples, GO enrichment analysis was conducted to annotate and classify the DEGs. The GO terms which have a relatively high count and small adjusted *P*-value are shown in Table 1, with a full list of the significantly enriched GO terms in Supplementary Table S8. Compared with T0, genes involved in lipid metabolic processes, cell wall, hydrolase activity—acting on glycosyl bonds [potentially playing a role in modifying plant cell wall architecture (Lopez-Casado *et al.*, 2008)]—and iron ion binding, all had higher expression in both T1 and T2. The up-regulation of genes involved in cell wall and iron ion binding could potentially be relevant to the binding of the foliar-absorbed Zn. In particular, 32 genes encoding multiorganism processes were also significantly up-regulated in T1, with this likely to be involved in the translocation of the Zn into the cells or organelles. In addition, the GO term 'response to wounding' was also significantly up-regulated in T1, suggesting that the foliar Zn application caused abiotic stress to the plant. In contrast, the genes encoding translation, the ATP metabolic process, and ribosome were all down-regulated in T1 and T2 compared with T0, implying that the fundamental metabolic activities were reduced in T1 and T2 (Table 1; Supplementary Table S8).

Next, DEGs were further annotated with the KEGG database to elucidate the molecular interactions of the DEGs among the samples. A full list of the significantly enriched KEGG pathways can be found in Supplementary Table S9. Similar results were found in the KEGG analysis with the GO enrichment. Specifically, compared with T0, the pathways relevant to fatty acid metabolism were both up-regulated in T1 and T2. In T1, pathways of plant–pathogen interaction and the mitogen-acivated protein kinase (MAPK) signalling pathway (could also be involved in plant responses to stress) (Danquah *et al.*, 2014) were also up-regulated; this is consistent with the GO analysis showing up-regulation for response to wounding in T1. In contrast, the biosynthesis of amino acids and ribosomes were both down-regulated in T1 and T2 (Supplementary Table S9).

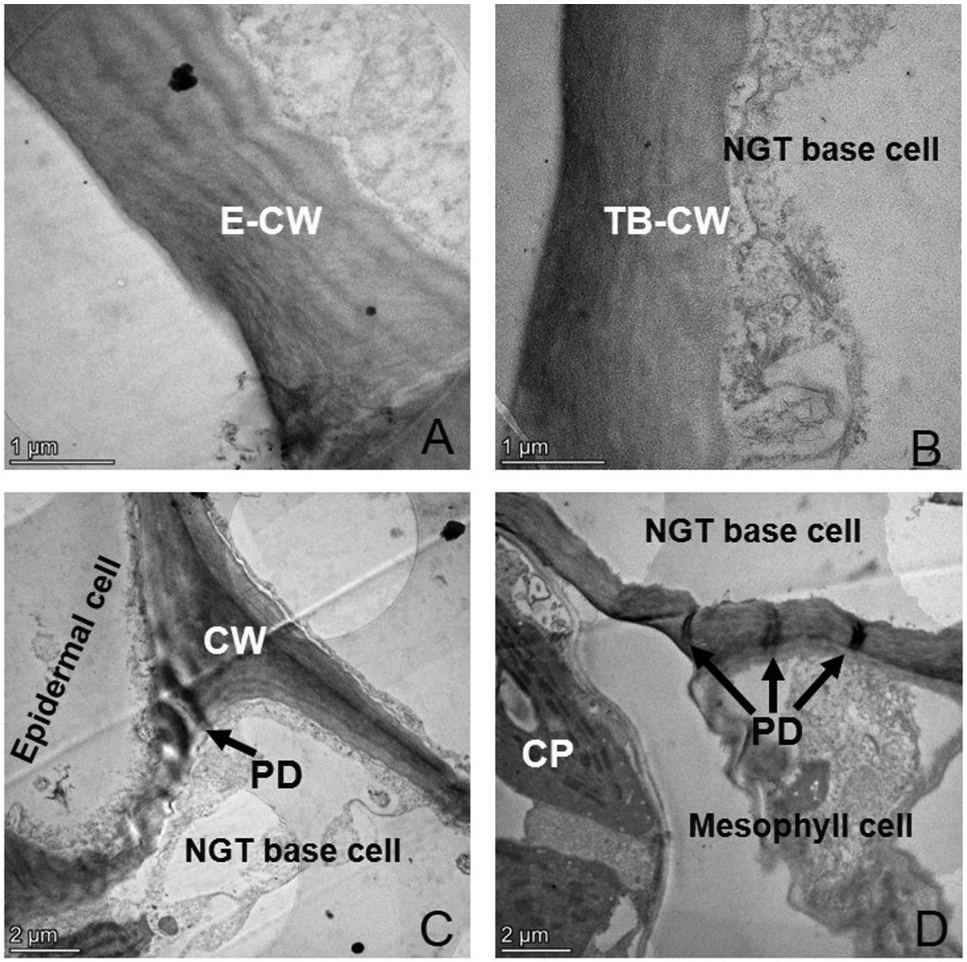

Fig. 4. Transmission electron micrographs from a cross-section of a sunflower leaf showing the basal cell of the NGTs. (A) Cell wall of a leaf epidermal cell and (B) cell wall of an NGT basal cell. (C) The NGT basal cell is connected to the adjacent epidermal cell with plasmodesmata, whilst (D) the epidermal cell is also connected with the underlying mesophyll cell. E-CW, combined cuticle and epidermal cell wall; TB-CW, combined cuticle and NGT base cell wall; PD, plasmodesmata; CP, chloroplast.

DGEs involved in heavy metal transporters and metal-chelating ligands

The movement of Zn in plant tissues, either as free Zn ions or as chelated Zn, is mediated by specialized transporters (Sinclair and Krämer, 2012). In the DEGs, nine transporter groups that are potentially involved in the translocation of Zn were identified, namely ATP-binding cassette (ABC) transporters, heavy metal-associated isoprenylated protein (HIPP), protein DETOXIFICATION (DTX), yellow stripe-like transporter (YSL), the ZRT/ IRT-like protein (ZIP), pleiotropic drug resistance protein (PDR), metal tolerance proteins (MTPs), heavy metal ATPase (HMA), and natural resistance-associated macrophage protein (Nramp). A full list of the DEGs of the nine transporter groups in the three samples is shown in Supplementary Table S10. A total of 120 DEGs of the nine groups were found (Fig. 6A), with 31.7% of them being ABC transporters, 26.7% being HIPP, 19.2% being DTX, and the remaining five groups all accounting for <7% each. For the 120 DEGs, 54% were up-regulated in T1 and/or T2 (Supplementary Table S10).

Metal-chelating ligands, including glutathione, metallothioneins (MTs), nicotianamine, histidine, cysteine, citrate, methionine, pectin, and heat shock protein (HSP), play important roles in plant Zn homeostasis (Martinka *et al.*, 2014). For example, upon a sudden increase of metal concentrations in plants, these ligands can function as buffers or chaperones to sequester and detoxify the metals (Hassinen *et al.*, 2007). Here, a total of 168 DEGs of these nine ligand groups were found, including 30.4% cysteine, 29.2% HSP, 20.8% glutathione, 6.5% histidine, and the remaining five categories all below 5% each (Fig. 6B). A full list of these DEGs can be found in Supplementary Table S11. Overall, a total of 61% (102) of the DEGs were up-regulated in T1 and/or T2, with over half of the glutathione, histidine, cysteine, citrate, HSP, and pectin up-regulated in T1 and/or T2.

qRT–PCR validation

To validate the different expression patterns observed in the RNA-Seq data, 15 DEGs were selected for qRT–PCR

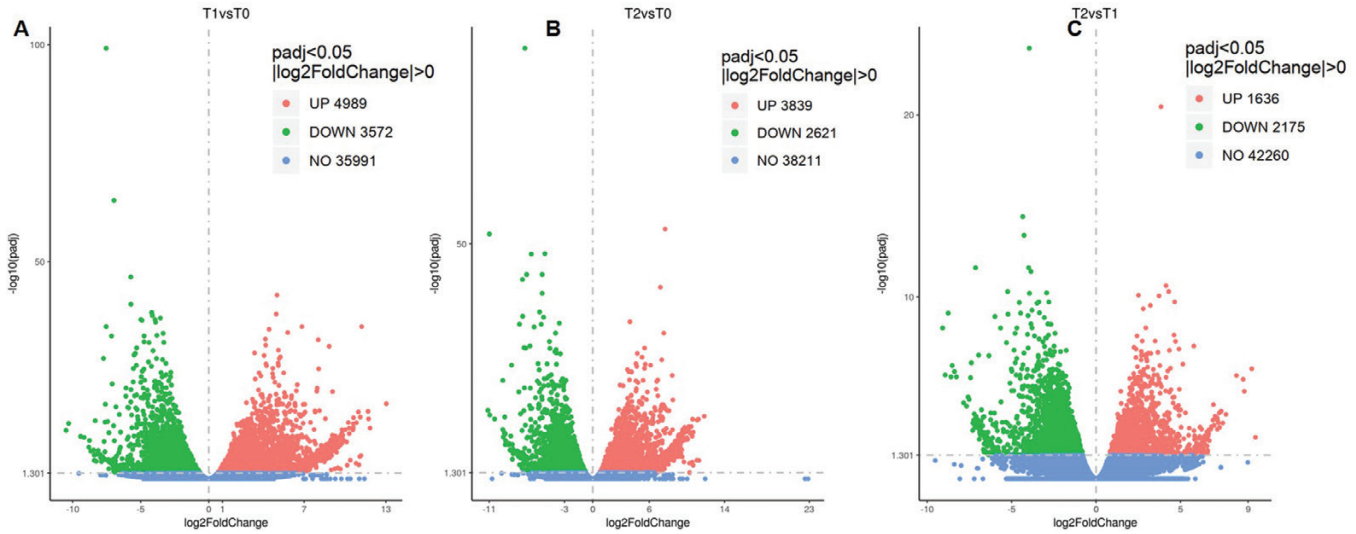

Fig. 5. Volcano plots of differentially expressed genes (DEGs). Volcano plots showing the DEGs between T1 and T0 (A), T2 and T0 (B), and T2 and T1 (C); in each plot, the red dots refer to the up-regulated genes, the green dots refer to the down-regulated genes, and the blue dots are the genes not differently expressed. T0 is NGTs collected from control leaves. T1 is NGTs collected from leaves after a 0.5 h Zn foliar application period. T2 is NGTs sampled from leaves 45 h after the 0.5 h Zn treatment period.

Table 1. Selected significantly enriched GO terms of the differentially expressed genes at T0, T1, and T2

Category	GO ID	Description	Adjusted *P*-value	Count
T1 versus T0 up-regulated				
BP	GO:0009611	Response to wounding	2.4E-07	11
BP	GO:0006629	Lipid metabolic process	0.0037	88
BP	GO:0051704	Multiorganism process	0.025	32
CC	GO:0005618	Cell wall	9.5E-08	29
MF	GO:0016798	Hydrolase activity, acting on glycosyl bonds	6.4E-13	102
MF	GO:0005506	Iron ion binding	6.1E-05	85
T2 versus T0 up-regulated				
BP	GO:0006629	Lipid metabolic process	0.0088	74
CC	GO:0005618	Cell wall	2.2E-05	24
MF	GO:0005506	Iron ion binding	4.9E-11	89
MF	GO:0016798	Hydrolase activity, acting on glycosyl bonds	1.2E-07	75
T1 versus T0 down-regulated				
BP	GO:0006412	Translation	3.4E-11	110
BP	GO:0006082	Organic acid metabolic process	1.1E-07	84
BP	GO:0046034	ATP metabolic process	1.4E-07	37
CC	GO:0005840	Ribosome	1.5E-09	87
MF	GO:0003735	Structural constituent of ribosome	1.9E-11	85
MF	GO:0015075	Ion transmembrane transporter activity	6.2E-05	66
T2 versus T0 down-regulated				
BP	GO:0043604	Amide biosynthetic process	5.4E-05	73
BP	GO:0006412	Translation	0.00012	69
BP	GO:0006757	ATP generation from ADP	0.0058	14
CC	GO:0043228	Non-membrane-bounded organelle	0.0268	59
MF	GO:0003735	Structural constituent of ribosome	1.8E-05	56

Adjusted *P*-value <0.05 is defined as significantly enriched; category refers to the function classification of the GO terms: biological process (BP), cellular component (CC), and molecular function (MF); count means the number of the DEGs assigned to this GO term.

examination. As shown in Supplementary Fig. S3, the expression patterns of all the selected genes were consistent with the results of the RNA-Seq analysis, demonstrating that the transcriptomic results are reliable and valid.

Discussion

As the outmost outgrowth on leaf surface, trichomes are potentially important in absorption of foliar-applied fertilizers, yet previous studies regarding foliar nutrient absorption pathway

investigation have focused almost exculsively on the cuticle and stomata (Schönherr and Luber, 2001; Schreiber, 2005; Chater *et al.*, 2014; Fernández *et al.*, 2017). Despite the fact that we have previously observed high concentrations of Zn accumulation in the NGTs of sunflower (Li *et al.*, 2019), it is unclear how Zn entered there and the fate of this Zn in the NGTs. The present study focused on the absorption and translocation of foliar-applied Zn in the NGTs of sunflower. After foliar application of Zn for only 0.5 h, we found that the Zn concentrations in the basal cells of NGTs were approximately three times higher than for the general cuticular areas (Fig. 2). Interestingly, even after removing the remaining Zn from the leaf surface and allowing the plant to continue growing, the Zn concentration in the NGTs continued to increase for a further 6 h before then decreasing. In contrast, for the general cuticular areas, although Zn had increased following the initial 0.5 h application, it began to decrease rapidly upon removal of Zn solution from the leaf surface (Fig. 2). Confocal Raman microscopy suggested that the cuticles of the NGT basal cells have a higher carbohydrate content than the general cuticle area (Fig. 3). Use of TEM showed that the NGT basal cells were connected to their surrounding cells by plasmodesmata (Fig. 4). In addition, transcriptome analyses showed that the foliar Zn application caused a significant up-regulation of genes involved in cell wall construction and iron ion binding in the NGTs (Table 1). In addition, nine groups of Zn transporters and Zn-chelating ligands were identified in the DEGs, including major changes for transporters (ABC transporters, HIPP, and DTX) and chelating ligands (cysteine, HSP, and glutathione) (Fig. 6). Overall, the present study found that Zn that accumulated in the NGTs was derived from both direct absorption and its subsequent translocation from the surrounding tissues. In addition, this Zn accumulation within the NGTs was found to be only temporary, with the Zn eventually moved out of the NGTs and translocated to other tissues. These observations suggest, for the first time, that due to their special structural, chemical, and molecular properties, the NGTs are an important pathway for absorption of the foliar-applied Zn fertilizer in sunflower, and the Zn in the NGTs can be translocated away from the NGT and used elsewhere by the plant.

Initial absorption of the foliar-applied Zn by the NGTs

The present study found that it is likely that the NGTs are a preferred absorption site for the foliar-applied Zn (Fig. 2). Initially, we hypothesized that this might be due to differences in the chemical composition or thickness of the cuticle and cell wall surrounding the NGT compared with that of the general epidermal cells. Whilst TEM showed that there were no differences in thickness (Fig. 4), confocal Raman microscopy demonstrated that the cuticle for the NGT basal area had a strong peak at 1080 cm^{-1} (Fig. 3), with this peak probably related to carbohydrates (Gierlinger, 2018). This is important given that a higher carbohydrate content in the cuticle leads to a higher hydrophilicity (Popp *et al.*, 2005; Fernández *et al.*, 2016, 2017). Furthermore, Schreel *et al.* (2020) found that the hydroscopic properties of trichomes on the veins of beech (*Fagus sylvatica*) are important in foliar water uptake. It has also been proposed that the microbial community in the phyllosphere differs around the trichomes, with this potentially producing biosurfactants and increasing permeability (Remus-Emsermann *et al.*, 2011; Schlechter *et al.*, 2019), although further research is required in this regard. Overall, it can be deduced that sunflower NGTs seem more hydrophilic compared with the surrounding cuticular areas, with this enabling an enhanced absorption of foliar-applied Zn within the NGTs.

Translocation and fate of the foliar-absorbed Zn in the NGTs

Not only did Zn accumulate in the NGTs during the initial 0.5 h Zn application period, but the concentration within

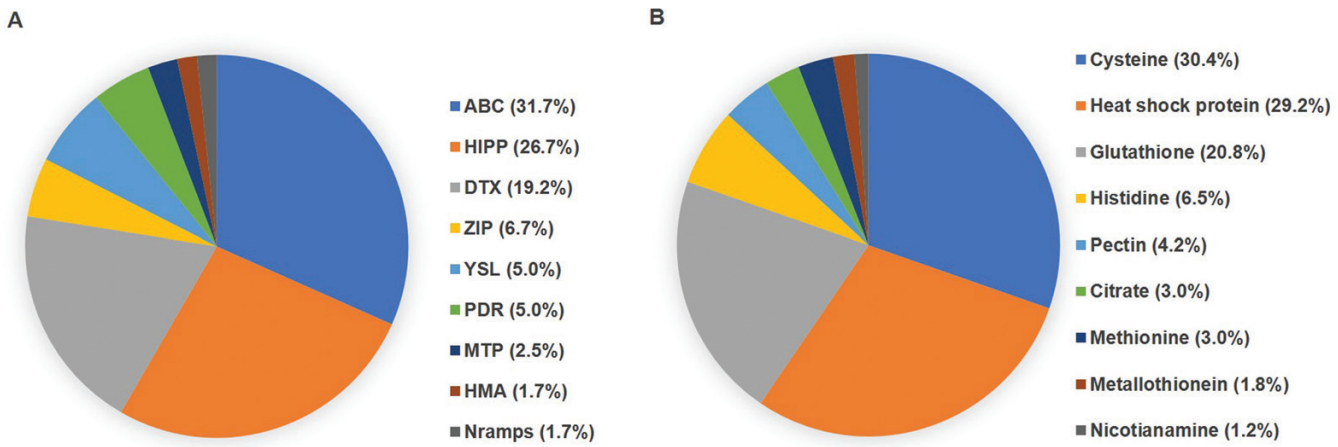

Fig. 6. The percentages of the DEGs in each category of heavy metal transporters (A) and metal-chelating ligands and protein (B) in T1 and/or T2 compared with T0.

the NGTs also continued to increase for a further 6 h even after the applied Zn was removed from the leaf surface (Fig. 2). Furthermore, Zn was also translocated into the abaxial NGTs in <3 h of initial foliar Zn application, despite the Zn being applied to the adaxial surface (Fig. 2; Supplementary Fig. S2). It is known that trichomes can play an important role in metal movement within plants. For example, the NGT basal cells in sunflower sequester excess manganese (Mn) supplied from the rooting medium, with this being an important mechanism for Mn tolerance (Blamey *et al.*, 1986, 2015). Indeed, the sequestration of various metals in leaf trichomes following their uptake from the rooting media has been reported for both hyperaccumulating and non-accumulating plants. For example, Zn and cadmium (Cd) accumulate in the hyperaccumulator plant *Arabidopsis helleri* (Küpper *et al.*, 2000; Zhao *et al.*, 2000), and Zn, lead (Pb), and Cd accumulate in the trichomes of *Alyssum montanum* (Muszynska *et al.*, 2018). It is generally assumed that the trichomes are functioning as a storage site for the detoxification of excess metals. Therefore, in the present study, it is possible that since the foliar application of Zn caused a sudden increase in the leaf Zn concentration, the plant moved excess Zn into the NGT base, thereby lowering the Zn concentration in the remainder of the leaf.

For foliar-applied Zn fertilizer, it is important to understand the fate of the Zn that accumulates in the NGTs, as this is relevant for determining the efficiency of the Zn fertilizer. It was found that the Zn concentration in the NGTs decreased gradually after 6 h following removal of the foliar-applied Zn (Fig. 2). Thus, there was a bidirectional translocation for the foliar-absorbed Zn in the NGTs: (i) Zn was sequestered in NGTs when the leaf Zn concentration was high; but (ii) it was subsequently translocated out of the NGTs once the leaf Zn concentration had then decreased.

Mechanism of the Zn accumulation and translocation in the NGTs: the role of the NGT basal cell walls

Our observation that the Zn translocated in the NGTs is supported by the observation that the NGT basal cell walls were connected to the surrounding cells by plasmodesmata (Fig. 4). Indeed, the GO enrichment found at T1 for genes involved in multiorganism processes was significantly up-regulated, with this process potentially relevant for the translocation of Zn between cells through the plasmodesmata. In addition, it has been reported previously that the base of the NGTs of sunflower are connected to the bundle sheath extensions, with it connecting with the vascular tissues (Li *et al.*, 2019). This explains the rapid translocation of Zn to the NGTs on the abaxial surface.

It is apparent from the XFM analyses (Supplementary Fig. S2) that the Zn accumulating at the base of the NGTs was probably within the cell wall (see also Li *et al.*, 2019). This is also observed in the other Zn foliar application studies (Doolette *et al.*, 2018; Xie *et al.*, 2020). Interestingly, following the foliar application of Zn in the present study, the genes in the NGTs coding for cell wall construction were significantly up-regulated. For example, GO terms of cell wall, xyloglucan:xyloglucosyl transferase activity, and hydrolase activity, acting on glycosyl bonds, were significantly up-regulated at both T1 and T2 compared with T0, with these terms all playing important roles in cell wall construction (Stratilova *et al.*, 2020). This cell wall reaction of the NGT base cells could be related to the Zn accumulating in the NGTs.

Mechanism of the Zn accumulation and translocation in the NGTs: the role of the Zn-chelating ligands and transporters in the NGTs

Nine groups of potential Zn transporters were identified in the DEGs, of which the ABC transporter, HIPP, and DTX accounted for 77.6% of the DEGs (Fig. 6A). ABC transporters can import nutrients and other molecules into cells or export toxins and lipids out of the cells (Rees *et al.*, 2009). In this regard, it has been reported that ABC transporters can be induced by excessive Zn in rice (*Oryza sativa*) (Moons, 2003). HIPP is a heavy metal-associated (HMA) isoprenylated plant protein that plays an important role in heavy metal homeostasis and detoxification mechanisms (de Abreu-Neto *et al.*, 2013). For example, HIPP was found to play an important role in Cd detoxification (Zhao *et al.*, 2013; Manara *et al.*, 2020). DTXs, which are protein DETOXIFICATION (Yu *et al.*, 2018) or detoxification efflux carriers (Ali *et al.*, 2021), are transporters belonging to the Multidrug and Toxic Compound Extrusion efflux (MATE) family, and provide a response to abiotic stresses such as drought, salt, and cold stress (Lu *et al.*, 2019), and detoxification of heavy metals (Dong *et al.*, 2019). These findings suggest that the ABC transporter, HIPP, and DTX could potentially be involved in Zn foliar absorption and translocation in the NGTs.

Furthermore, nine groups of ligands were identified in the DEGs, with cysteine, HSP, and glutathione together accounting for 80% of the nine groups (Fig. 6B). The DEGs related to cysteine had the highest proportion among the nine groups, suggesting that cysteine has a strong response upon foliar application of Zn. These findings are in agreement with those of Domínguez-Solís *et al.* (2004) who found that cysteine availability is essential for Cd tolerance in *Arabidopsis thaliana*, with most Cd accumulated in its leaf trichomes. Cysteine is the precursor molecule for the synthesis of glutathione, a compound of great importance as cellular defence against heavy metal and oxidative stress (Miot *et al.*, 2008; Asgher *et al.*, 2017; Kim *et al.*, 2017). A total of 49 DEGs of HSPs were also identified, with most of these being for HSP70. This is also in agreement with other transcript analyses showing that HSP70 is highly expressed under a variety of metal stresses (Hasan *et al.*, 2017). Therefore, the data suggest that cysteine, glutathione, and HSP are also

related to Zn accumulation and translocation in the NGTs. The present study provides valuable information for understanding the molecular mechanism of trichome foliar Zn absorption and to further examine the functions of individual interesting genes.

Finally, it must be noted that trichomes vary greatly in their structure and function, and hence not all trichomes are important for absorption and translocation of foliar-applied fertilizers. For example, the two other types of trichomes in sunflower (Fig. 1) and the trichomes of soybean (*Glycine max*) have been shown to have no special role in the absorption and translocation of foliar-applied Zn fertilizers (Li *et al.*, 2018*a*). The findings of the present study suggest that trichomes having the following characteristics potentially play a role in the absorption and translocation of foliar-applied nutrients, namely having a cuticle with a high hydrophilicity, with base cells that are well connected with the surrounding tissues via bundle sheath extensions and plasmodesmata, and having abundant metal-chelating ligands and transporters. Regardless, our findings suggest that plants that have trichomes possessing those characteristics would show a higher efficiency for foliar fertilization given that their trichomes not only facilitate the absorption but also play an important role in regulating the translocation of these foliar-absorbed nutrients.

Conclusions

We have demonstrated that the NGTs of sunflower are important for the absorption of foliar-applied Zn. Furthermore, not only were the NGTs likely to be an important pathway for the initial absorption of the foliar-applied Zn, but they are also a Zn-buffering site within the leaf. Specifically, Zn is translocated into the NGT base when the leaf Zn concentration is high (i.e. during the initial Zn foliar absorption stages) but is subsequently translocated out of the NGTs when the leaf Zn concentration decreases. These observations are likely to be due to the special chemical, structural, and molecular properties of the NGTs, such as the cuticle composition and cell structure at their base, and the Zn-chelating ligands and transporters in the NGTs. This study demonstrates for the first time that NGTs have a key structural and functional role in the absorption and translocation of foliar-applied Zn.

Supplementary data

The following supplementary data are available at *JXB* online.

Fig. S1. Images showing the set-up for the time-resolved XFM analysis on the living sunflower plant.

Fig. S2. Differentiation of the non-glandular trichomes (NGTs) on the adaxial and abaxial leaf side of sunflower.

Fig. S3. qRT–PCR validation results.

Table S1. Previous studies reporting that leaf trichomes can absorb water.

Table S2. Primers used for qRT–PCR.

Table S3. Overview of RNA sequencing results and data quality assessment.

Table S4. Mapping rates of the clean reads aligned to the genome of sunflower.

Table S5. Pearson correlation (R^2) between samples (calculated based on the FPKM values of each sample).

Table S6. List of the FPKM value of all the genes in the sample libraries.

Table S7. List of the DEGs identified in T1 and/or T2 compared with T0.

Table S8. List of the significantly enriched GO terms among the DEGs.

Table S9. List of the significantly enriched KEGG pathway terms among the DEGs.

Table S10. List of the DEGs of the potential Zn transporters in T0, T1, and T2.

Table S11. List of the DEGs of the metal-chelating ligands and proteins in T0, T1, and T2.

Acknowledgements

The authors acknowledge use of the facilities and technical assistance of the Analytical & Testing Centre of the Northwestern Polytechnical University. Parts of the research were undertaken on the XFM beamline (13412) at the Australian Synchrotron, part of the Australian Nuclear Science and Technology Organisation (ANSTO). This work was supported by a China Postdoctoral Science Foundation grant (2019M663825), the Key Research and Development Program of Shaanxi Province (2019KW-044), the Fundamental Research Funds for the Central Universities of China (3102019JC007), and the National Natural Science Foundation of China (NSFC, 42077352). Support was also provided to CL through the International Postdoctoral Exchange Fellowship Program (Talent-Introduction Program, YJ20190217).

Author contributions

CL and PMK: conceptualization and data curation; CL, PMK, JTW, and LLW: formal analysis; CL, PMK, JTW, LLW, and FPCB: investigation; CL, PMK, JTW, LLW, FPCB, LNZ, DJP, AVDE, VF, and EL: methodology; CL and PMK: writing—original draft; CL, FPBC, AVDE, VF, EL, YHW, and PMK: writing—review and editing; YHW, CL, and PMK: funding acquisition; DJP: resources; PMK and YHW: supervision.

Data availability

All data supporting the findings of this study are available within the paper and the supplementary data published online.

References

Ali E, Saand MA, Khan AR, Shah JM, Feng S, Ming C, Sun P. 2021. Genome-wide identification and expression analysis of detoxification efflux carriers (DTX) genes family under abiotic stresses in flax. Physiologia Plantarum **171**, 483–501.

Aschenbrenner A-K, Horakh S, Spring O. 2013. Linear glandular trichomes of *Helianthus* (Asteraceae): morphology, localization, metabolite activity and occurrence. AoB Plants **5**, plt028.

Asgher M, Per TS, Anjum S, Khan MIR, Masood A, Verma S, Khan NA. 2017. Contribution of glutathione in heavy metal stress tolerance in plants. In: Khan MIR, Khan NA, eds. Reactive oxygen species and antioxidant systems in plants: role and regulation under abiotic stress. Singapore: Springer Singapore, 297–313.

Badouin H, Gouzy J, Grassa CJ, *et al.* 2017. The sunflower genome provides insights into oil metabolism, flowering and Asterid evolution. Nature **546**, 148–152.

Balcke GU, Bennewitz S, Bergau N, Athmer B, Henning A, Majovsky P, Jiménez-Gómez JM, Hoehenwarter W, Tissier A. 2017. Multi-omics of tomato glandular trichomes reveals distinct features of central carbon metabolism supporting high productivity of specialized metabolites. The Plant Cell **29**, 960–983.

Benzing DH, Henderson K, Kessel B, Sulak J. 1976. Absorptive capacities of bromeliad trichomes. American Journal of Botany **63**, 1009–1014.

Bickford CP. 2016. Ecophysiology of leaf trichomes. Functional Plant Biology **43**, 807–814.

Blamey FP, Hernandez-Soriano MC, Cheng M, Tang C, Paterson DJ, Lombi E, Wang WH, Scheckel KG, Kopittke PM. 2015. Synchrotron-based techniques shed light on mechanisms of plant sensitivity and tolerance to high manganese in the root environment. Plant Physiology **169**, 2006–2020.

Blamey FPC, Joyce DC, Edwards DG, Asher CJ. 1986. Role of trichomes in sunflower tolerance to manganese toxicity. Plant and Soil **91**, 171–180.

Chater CCC, Oliver J, Casson S, Gray JE. 2014. Putting the brakes on: abscisic acid as a central environmental regulator of stomatal development. New Phytologist **202**, 376–391.

Dalin P, Ågren J, Björkman C, Huttunen P, Kärkkäinen K. 2008. Leaf trichome formation and plant resistance to herbivory. In: Schaller A, ed. Induced plant resistance to herbivory. Cham: Springer, 89–105.

Danquah A, de Zelicourt A, Colcombet J, Hirt H. 2014. The role of ABA and MAPK signaling pathways in plant abiotic stress responses. Biotechnology Advances **32**, 40–52.

de Abreu-Neto JB, Turchetto-Zolet AC, de Oliveira LFV, Bodanese Zanettini MH, Margis-Pinheiro M. 2013. Heavy metal-associated isoprenylated plant protein (HIPP): characterization of a family of proteins exclusive to plants. The FEBS Journal **280**, 1604–1616.

Domínguez-Solís JR, López-Martín MC, Ager FJ, Ynsa MD, Romero LC, Gotor C. 2004. Increased cysteine availability is essential for cadmium tolerance and accumulation in *Arabidopsis thaliana*. Plant Biotechnology Journal **2**, 469–476.

Dong B, Niu L, Meng D, Song Z, Wang L, Jian Y, Fan X, Dong M, Yang Q, Fu Y. 2019. Genome-wide analysis of MATE transporters and response to metal stress in *Cajanus cajan*. Journal of Plant Interactions **14**, 265–275.

Doolette CL, Read TL, Li C, Scheckel KG, Donner E, Kopittke PM, Schjoerring JK, Lombi E. 2018. Foliar application of zinc sulphate and zinc EDTA to wheat leaves: differences in mobility, distribution, and speciation. Journal of Experimental Botany **69**, 4469–4481.

Eichert T, Goldbach H, Burkhardt J. 1998. Evidence for the uptake of large anions through stomatal pores. Botanica Acta **111**, 461–466.

Eichert T, Kurtz A, Steiner U, Goldbach HE. 2008. Size exclusion limits and lateral heterogeneity of the stomatal foliar uptake pathway for aqueous solutes and water-suspended nanoparticles. Physiologia Plantarum **134**, 151–160.

Fernandez P, Di Rienzo J, Fernandez L, Hopp HE, Paniego N, Heinz RA. 2008. Transcriptomic identification of candidate genes involved in sunflower responses to chilling and salt stresses based on cDNA microarray analysis. BMC Plant Biology **8**, 11.

Fernández V, Bahamonde HA, Javier Peguero-Pina J, Gil-Pelegrín E, Sancho-Knapik D, Gil L, Goldbach HE, Eichert T. 2017. Physicochemical properties of plant cuticles and their functional and ecological significance. Journal of Experimental Botany **68**, 5293–5306.

Fernández V, Guzmán-Delgado P, Graça J, Santos S, Gil L. 2016. Cuticle structure in relation to chemical composition: re-assessing the prevailing model. Frontiers in Plant Science **7**, 427.

Fernández V, Sancho-Knapik D, Guzmán P, *et al.* 2014. Wettability, polarity, and water absorption of holm oak leaves: effect of leaf side and age. Plant Physiology **166**, 168–180.

Fernández V, Sotiropoulos T, Brown P. 2013. Foliar fertilization: scientific principles and field practices. Paris: International Fertilizer Industry Association (IFA), 12–70.

Gierlinger N. 2018. New insights into plant cell walls by vibrational microspectroscopy. Applied Spectroscopy Reviews **53**, 517–551.

Gierlinger N, Schwanninger M. 2006. Chemical imaging of poplar wood cell walls by confocal Raman microscopy. Plant Physiology **140**, 1246–1254.

Greene PR, Bain CD. 2005. Total internal reflection Raman spectroscopy of barley leaf epicuticular waxes *in vivo*. Colloids and Surfaces B: Biointerfaces **45**, 174–180.

Griss E. 1844. Nouvelles experiences sur l'action des composés ferrugineux soluble, appliques e la vegetation, et specialement au traitament de la chlorosees, et de la débilité des plantes. Comptes Rendus de l'Académie des Sciences **19**, 1118–1119.

Hasan MK, Cheng Y, Kanwar MK, Chu XY, Ahammed GJ, Qi ZY. 2017. Responses of plant proteins to heavy metal stress—a review. Frontiers in Plant Science **8**, 1492.

Hassinen VH, Tervahauta AI, Halimaa P, Plessl M, Peräniemi S, Schat H, Aarts MG, Servomaa K, Kärenlampi SO. 2007. Isolation of Zn-responsive genes from two accessions of the hyperaccumulator plant *Thlaspi caerulescens*. Planta **225**, 977–989.

Herppich WB, Martin CE, Tötzke C, Manke I, Kardjilov N. 2019. External water transport is more important than vascular transport in the extreme atmospheric epiphyte *Tillandsia usneoides* (Spanish moss). Plant, Cell & Environment **42**, 1645–1656.

Holanda AER, Souza BC, Carvalho ECD, Oliveira RS, Martins FR, Muniz CR, Costa RC, Soares AA. 2019. How do leaf wetting events affect gas exchange and leaf lifespan of plants from seasonally dry tropical vegetation? Plant Biology **21**, 1097–1109.

Hunt M, Kaur N, Stromvik M, Vodkin L. 2011. Transcript profiling reveals expression differences in wild-type and glabrous soybean lines. BMC Plant Biology **11**, 145.

Ju J, Bai H, Zheng Y, Zhao T, Fang R, Jiang L. 2012. A multi-structural and multi-functional integrated fog collection system in cactus. Nature Communications **3**, 1247.

Kim YO, Bae HJ, Cho E, Kang H. 2017. Exogenous glutathione enhances mercury tolerance by inhibiting mercury entry into plant cells. Frontiers in Plant Science **8**, 683.

Kopittke PM, Menzies NW, de Jonge MD, *et al.* 2011. *In situ* distribution and speciation of toxic copper, nickel, and zinc in hydrated roots of cowpea. Plant Physiology **156**, 663–673.

Küpper H, Lombi E, Zhao FJ, McGrath SP. 2000. Cellular compartmentation of cadmium and zinc in relation to other elements in the hyperaccumulator *Arabidopsis halleri*. Planta **212**, 75–84.

Levin DA. 1973. Role of trichomes in plant denfense. Quarterly Review of Biology **48**, 3–15.

Li C, Wang P, Lombi E, Cheng M, Tang C, Howard DL, Menzies NW, Kopittke PM. 2018*a*. Absorption of foliar-applied Zn fertilizers by trichomes in soybean and tomato. Journal of Experimental Botany **69**, 2717–2729.

Li C, Wang P, Lombi E, Wu J, Blamey FPC, Fernández V, Howard DL, Menzies NW, Kopittke PM. 2018*b*. Absorption of foliar applied Zn is decreased in Zn deficient sunflower (*Helianthus annuus*) due to changes in leaf properties. Plant and Soil **433**, 309–322.

Li C, Wang P, van der Ent A, *et al.* 2019. Absorption of foliar-applied Zn in sunflower (*Helianthus annuus*): importance of the cuticle, stomata and trichomes. Annals of Botany **123**, 57–68.

Livak KJ, Schmittgen TD. 2001. Analysis of relative gene expression data using real-time quantitative PCR and the $2^{-\Delta\Delta CT}$ method. Methods **25**, 402–408.

Lopez-Casado G, Urbanowicz BR, Damasceno CM, Rose JK. 2008. Plant glycosyl hydrolases and biofuels: a natural marriage. Current Opinion in Plant Biology **11**, 329–337.

Lu P, Magwanga RO, Kirungu JN, *et al.* 2019. Overexpression of cotton a *DTX/MATE* gene enhances drought, salt, and cold stress tolerance in transgenic arabidopsis. Frontiers in Plant Science **10**, 299.

Manara A, Fasani E, Molesini B, DalCorso G, Pennisi F, Pandolfini T, Furini A. 2020. The tomato metallocarboxypeptidase inhibitor 1, which interacts with a heavy metal-associated isoprenylated protein, is implicated in plant response to cadmium. Molecules **25**, 700.

Martin CE, Rux G, Herppich WB. 2013. Responses of epidermal cell turgor pressure and photosynthetic activity of leaves of the atmospheric epiphyte *Tillandsia usneoides* (Bromeliaceae) after exposure to high humidity. Journal of Plant Physiology **170**, 70–73.

Martinka M, Vaculik M, Lux A. 2014. Plant cell responses to cadmium and zinc. In: Nick P, Opatrny Z, eds. Applied plant cell biology, **Vol. 22**. Berlin Heidelberg: Springer, 209–246.

Miot J, Morin G, Skouri-Panet F, Férard C, Aubry E, Briand J, Wang Y, Ona-Nguema G, Guyot F, Brown GE. 2008. XAS study of arsenic coordination in *Euglena gracilis* exposed to arsenite. Environmental Science & Technology **42**, 5342–5347.

Moons A. 2003. *Ospdr9*, which encodes a PDR-type ABC transporter, is induced by heavy metals, hypoxic stress and redox perturbations in rice roots. FEBS Letters **553**, 370–376.

Muszyńska E, Labudda M, Różańska E, Hanus-Fajerska E, Znojek E. 2018. Heavy metal tolerance in contrasting ecotypes of *Alyssum montanum*. Ecotoxicology and Environmental Safety **161**, 305–317.

Nautiyal AK, Gani U, Sharma P, Kundan M, Fayaz M, Lattoo SK, Misra P. 2020. Comprehensive transcriptome analysis provides insights into metabolic and gene regulatory networks in trichomes of *Nicotiana tabacum*. Plant Molecular Biology **102**, 625–644.

Ohrui T, Nobira H, Sakata Y, *et al.* 2007. Foliar trichome- and aquaporin-aided water uptake in a drought-resistant epiphyte *Tillandsia ionantha* Planchon. Planta **227**, 47–56.

Paterson D, De Jonge M, Howard D, Lewis W, McKinlay J, Starritt A, Kusel M, Ryan C, Kirkham R, Moorhead G. 2011. The X-ray fluorescence microscopy beamline at the Australian Synchrotron. AIP Conference Proceedings **1365**, 219–222.

Pina ALCB, Zandavalli RB, Oliveira RS, Martins FR, Soares AA. 2016. Dew absorption by the leaf trichomes of *Combretum leprosum* in the Brazilian semiarid region. Functional Plant Biology **43**, 851–861.

Popp C, Burghardt M, Friedmann A, Riederer M. 2005. Characterization of hydrophilic and lipophilic pathways of *Hedera helix* L. cuticular membranes: permeation of water and uncharged organic compounds. Journal of Experimental Botany **56**, 2797–2806.

Ramu VS, Paramanantham A, Ramegowda V, Mohan-Raju B, Udayakumar M, Senthil-Kumar M. 2016. Transcriptome analysis of sunflower genotypes with contrasting oxidative stress tolerance reveals individual—and combined—biotic and abiotic stress tolerance mechanisms. PLoS One **11**, e0157522.

Rees DC, Johnson E, Lewinson O. 2009. ABC transporters: the power to change. Nature Reviews. Molecular Cell Biology **10**, 218–227.

Remus-Emsermann MN, de Oliveira S, Schreiber L, Leveau JH. 2011. Quantification of lateral heterogeneity in carbohydrate permeability of isolated plant leaf cuticles. Frontiers in Microbiology **2**, 197.

Reuveni R, Agapov V, Reuveni M, Raviv M. 1994. Effects of foliar sprays of phosphates on powdery mildew (*Sphaerotheca pannosa*) of roses. Journal of Phytopathology **142**, 331–337.

Ryan C. 2000. Quantitative trace element imaging using PIXE and the nuclear microprobe. International Journal of Imaging Systems and Technology **11**, 219–230.

Ryan C, Jamieson D. 1993. Dynamic analysis: on-line quantitative PIXE microanalysis and its use in overlap-resolved elemental mapping. Nuclear Instruments and Methods in Physics Research Section B **77**, 203–214.

Schilmiller AL, Last RL, Pichersky E. 2008. Harnessing plant trichome biochemistry for the production of useful compounds. The Plant Journal **54**, 702–711.

Schlechter RO, Miebach M, Remus-Emsermann MNP. 2019. Driving factors of epiphytic bacterial communities: a review. Journal of Advanced Research **19**, 57–65.

Schönherr J, Luber M. 2001. Cuticular penetration of potassium salts: effects of humidity, anions, and temperature. Plant and Soil **236**, 117–122.

Schrader B, Schulz H, Baranska M, Andreev GN, Lehner C, Sawatzki J. 2005. Non-destructive Raman analyses—polyacetylenes in plants. Spectrochimica Acta Part A **61**, 1395–1401.

Schreel JDM, Leroux O, Goossens W, Brodersen C, Rubinstein A, Steppe K. 2020. Identifying the pathways for foliar water uptake in beech (*Fagus sylvatica* L.): a major role for trichomes. The Plant Journal **103**, 769–780.

Schreiber L. 2005. Polar paths of diffusion across plant cuticles: new evidence for an old hypothesis. Annals of Botany **95**, 1069–1073.

Sinclair SA, Krämer U. 2012. The zinc homeostasis network of land plants. Biochimica et Biophysica Acta **1823**, 1553–1567.

Stratilová B, Šesták S, Mravec J, *et al.* 2020. Another building block in the plant cell wall: barley xyloglucan xyloglucosyl transferases link covalently xyloglucan and anionic oligosaccharides derived from pectin. The Plant Journal **104**, 752–767.

Vitarelli NC, Riina R, Cassino MF, Meira RMSA. 2016. Trichome-like emergences in *Croton* of Brazilian highland rock outcrops: evidences for atmospheric water uptake. Perspectives in Plant Ecology, Evolution and Systematics **22**, 23–35.

Vu DT, Huang L, V Nguyen A, Du Y, Xu Z, A Hampton M, Li P, Rudolph V. 2013. Quantitative methods for estimating foliar uptake of zinc from suspension-based Zn chemicals. Journal of Plant Nutrition and Soil Science **176**, 764–775.

Werker E. 2000. Trichome diversity and development. Advances in Botanical Research **31**, 1–35.

Xie R, Zhao J, Lu L, Brown P, Guo J, Tian S. 2020. Penetration of foliar-applied Zn and its impact on apple plant nutrition status: in vivo evaluation by synchrotron-based X-ray fluorescence microscopy. Horticulture Research **7**, 147.

Yan A, Pan J, An L, Gan Y, Feng H. 2012. The responses of trichome mutants to enhanced ultraviolet-B radiation in *Arabidopsis thaliana*. Journal of Photochemistry and Photobiology B: Biology **113**, 29–35.

Yu MM, Schulze HG, Jetter R, Blades MW, Turner RF. 2007. Raman microspectroscopic analysis of triterpenoids found in plant cuticles. Applied Spectroscopy **61**, 32–37.

Yu RG, Ma YY, Li Y, Li X, Liu CF, Du XL, Shi GR. 2018. Comparative transcriptome analysis revealed key factors for differential cadmium transport and retention in roots of two contrasting peanut cultivars. BMC Genomics **19**, 16.

Yue C, Cao HL, Chen D, Lin HZ, Wang Z, Hu J, Yang GY, Guo YQ, Ye NX, Hao XY. 2018. Comparative transcriptome study of hairy and hairless tea plant (*Camellia sinensis*) shoots. Journal of Plant Physiology **229**, 41–52.

Zhao F, Lombi E, Breedon T. 2000. Zinc hyperaccumulation and cellular distribution in *Arabidopsis halleri*. Plant, Cell & Environment **23**, 507–514.

Zhao J, Zhou H, Li X. 2013. UBIQUITIN-SPECIFIC PROTEASE16 interacts with a HEAVY METAL ASSOCIATED ISOPRENYLATED PLANT PROTEIN27 and modulates cadmium tolerance. Plant Signaling & Behavior **8**, e25680.